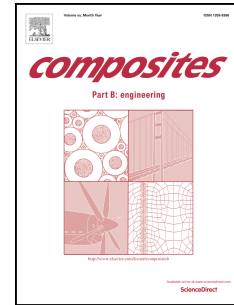


# Accepted Manuscript

Piezoresistive properties of resin reinforced with carbon nanotubes for health-monitoring of aircraft primary structures

L. Vertuccio, L. Guadagno, G. Spinelli, P. Lamberti, V. Tucci, S. Russo



PII: S1359-8368(16)31190-8

DOI: [10.1016/j.compositesb.2016.09.061](https://doi.org/10.1016/j.compositesb.2016.09.061)

Reference: JCOMB 4553

To appear in: *Composites Part B*

Received Date: 1 July 2016

Revised Date: 21 August 2016

Accepted Date: 20 September 2016

Please cite this article as: Vertuccio L, Guadagno L, Spinelli G, Lamberti P, Tucci V, Russo S, Piezoresistive properties of resin reinforced with carbon nanotubes for health-monitoring of aircraft primary structures, *Composites Part B* (2016), doi: 10.1016/j.compositesb.2016.09.061.

This is a PDF file of an unedited manuscript that has been accepted for publication. As a service to our customers we are providing this early version of the manuscript. The manuscript will undergo copyediting, typesetting, and review of the resulting proof before it is published in its final form. Please note that during the production process errors may be discovered which could affect the content, and all legal disclaimers that apply to the journal pertain.

## Piezoresistive Properties of Resin Reinforced with Carbon Nanotubes for Health-Monitoring of Aircraft Primary Structures

L. Vertuccio<sup>a\*</sup>, L. Guadagno<sup>a</sup>, G. Spinelli<sup>b</sup>, P. Lamberti<sup>b</sup>, V. Tucci<sup>b</sup>, S. Russo<sup>c</sup>

<sup>a</sup> Department of Industrial Engineering University of Salerno, Via Giovanni Paolo II, Fisciano (SA)  
ITALY

<sup>b</sup> Department of Information and Electrical Engineering and Applied Mathematics University of Salerno,  
Via Giovanni Paolo II, Fisciano (SA) ITALY

<sup>c</sup> Finmeccanica SpA, Engineering and Industrialization / New Airframe Technologies Viale  
dell'Aeronautica, Pomigliano D'Arco (NA), 80038, Italy

\**lvertuccio@unisa.it; lguadagno@unisa.it; gspinelli@unisa.it; plamberti@unisa.it; vtucci@unis.it;*  
*salvatore.russo@finmeccanica.com*

### Abstract

A study concerning the development of embedded sensors by using polymer composite filled with carbon nanotube for structural health monitoring in aeronautic structural parts is presented. The relationship between the mechanical stress applied, both in axial and flexural mode and the electrical properties of an epoxy composite, are analyzed. The electrical resistance or impedance of the nanocomposites samples are strongly affected by the applied mechanical stress. The present work aims at investigating the possible use of the nanotechnology towards the development of embedded sensor systems in composite structures having self-diagnostic functionalities and capability of provide real-time structural health monitoring.

### Keywords:

- A. Carbon-carbon composites (CCCs)
- A. Smart materials
- B. Electrical properties
- D. Mechanical testing

## 1. Introduction

Lightweight composites based on thermosetting and thermoplastic polymers reinforced with different carbon nanoparticles, such as Carbon Nanotubes (CNT), are increasingly adopted for the fabrication of multifunctional components in different industrial sectors, such as aeronautic, automotive, etc. For example, nanocomposites based on thermosetting resins are replacing traditional materials in structural applications due to their high fracture toughness against impact damages, easy processability and shaping possibilities, resistance to several aggressive environments (corrosion, flame, moisture, etc.). The inclusion of CNT even at low weight concentrations, due to their tendency to easily form electrically conductive networks, may also impart piezo-resistive properties to the resulting nanostructured composite thus leading to a multifunctional component integrating structural and sensing capabilities [1-5]. In fact, a correlation between the reversible mechanical deformations and the electrical resistance of CNT-based composites has been found making them suitable for use as strain (or stress) sensors [6, 7]. Moreover, filled polymers can be designed to have specific and tailored properties, thus offering many advantages in comparison to conventional materials based on electro-active polymers or piezoelectric ceramics which present different limitations due to their fragility, non-negligible weight and high voltage or current required for their proper use. Therefore, nanocomposites able to measure their own strains through variation in electrical resistance even at very low operating voltage, lead to the availability of sensor with customized features, design flexibilities and employable even in very harsh environments [8, 9]. These remarkable features are particularly attractive in aeronautic components where the stress/strain sensors play a crucial role for structural health monitoring (SHM) of fundamental parts of aircrafts (i.e. fuselage, wings, cockpit) constantly exposed to threatening environmental effects such as temperature changes, impact by birds or hailstones, lightning strikes, etc. that may affect the safety, serviceability and reliability of the vehicles [10-12].

The classical real-time sensing approach in these applications, based on piezoresistive material placed on the monitored structure surface and on the detection of the strain-induced electric charge or current, typically suffer from high cost, small sensing area, low durability. In addition, as it concerns the land inspections, expensive and time consuming X-ray and ultrasonic techniques, and acceleration-based modal testing are employed. Strain sensors embedded in a composite structure may allow to overcome such drawbacks providing efficient structural health monitoring, improved durability and reliability and reduced inspection and maintenance costs of composite structures [13]. Although the strain sensing characteristics of composites reinforced with carbon nanofillers have been successfully employed in

different studies, some critical issues related to material choice and fabrication processes need further investigations. In particular, the non-uniform dispersion of CNT in the resin may introduce entangled aggregates which in turn impact on the sensing performances, the CNT/matrix interactions may affect the load transfer between the two phases, as well as the electrical, thermal, and piezoresistive properties of the nanocomposite. For these reasons different simulation and experimental measurements have been carried out in order to analyze the effect of processing parameters and material properties on sensitivity of the resulting nanocomposites [4, 14]. The piezoresistive response of thick-film epoxy-graphite composite materials has been studied with particular emphasis on the effect of graphite particle size on the resistance values, due to the tunneling effect. [15]. Moreover, the behavior under tension and compression of a vinyl ester thermosetting resin filled with multi-walled carbon nanotubes has been studied under both elastic and plastic deformations [16]. Recently a comprehensive review on the recent technological advances of stretchable, skin-mountable, and wearable strain sensor was reported in order to understand the physical phenomenon behind the piezoresistive properties of innovative and smart materials [17]. Furthermore the frequency dependent electrical response of a nanocomposite to a mechanical strain and its variability with filler loading has been analyzed [18, 19]. However, most of the available works scrutinize the strain sensing properties of the nanocomposites on the basis of DC electrical characterizations, while only a few deal with AC measurements [20-23]. Hence, in this paper the DC and AC response of specimens of an aeronautical epoxy resin loaded with 0.3 %wt of multi-walled (MWCNT) stressed in axial and flexural mode is investigated. More in details, the variations of the electrical resistance or impedance that occur during the mechanical stresses are correlated to the structural deformation exhibited by the composites. The morphological characteristics of the considered composite system are accurately investigated by different techniques in order to achieve a deep knowledge of the structural ordering and the bonding states of carbons in the nanotube structures. The mechano-electrical tests show that the response of the composite is characterized by a linear increase of the electrical resistance with the strain at least in the region of elastic deformation of the material. Moreover, it is found that the composite exhibits a higher sensitivity as the frequency increases. The sensing characteristics of the nanocomposites are explained in terms of the mechanisms affecting mechanical-electrical response the percolation network formed by the MWCNT. The optimal operation conditions of these stimuli-responsive materials for structural aircraft monitoring applications are also discussed.

## 2. Experimental

### 2.1 Materials

The epoxy matrix was prepared by mixing an epoxy precursor, tetraglycidyl methylene dianiline (TGMDA) with an epoxy reactive monomer 1, 4-butanediol diglycidyl ether (BDE) that acts as a reactive diluent. The curing agent adopted for this manufacturing process is 4, 4-diaminodiphenyl sulfone (DDS). The epoxy mixture was obtained by mixing TGMDA with BDE monomer at a concentration of 80:20% (by weight) epoxide to flexibilizer. The hardener agent was added at a stoichiometric concentration with respect to all the epoxy rings (TGMDA and BDE). This particular epoxy formulation has proven to be very effective for improving nanofiller dispersion due to a decrease in the viscosity [24, 25]. In addition, it has been found to reduce the moisture content which is a very critical characteristic for aeronautic materials [26]. Moreover, this epoxy formulation hardened with DDS is characterized by a good flame resistance with a limiting oxygen index of 27%, even without addition of ant flame compounds [27]. Epoxy blend and DDS were mixed at 120 °C and the MWCNT (3100 Grade purchased from Nanocyl S.A) were added and incorporated into the matrix by using an ultrasonication for 20 min (Hielscher model UP200S-24 kHz high power ultrasonic probe) in order to obtain a homogeneous dispersion. All the mixtures were cured by a two-stage curing cycles: a first isothermal stage was carried out at the lower temperature of 125 °C for 1 hour and the second isothermal stage at higher temperatures up to 180 °C or 200 °C for 3 hours.

### 2.2 Characterization

#### 2.2.1 Raman analysis

Raman spectra were obtained at room temperature with a micro-Raman spectrometer Renishaw inVia with a 514 nm excitation wavelength (laser power 30 mW) in the range 100–3000  $\text{cm}^{-1}$ .

#### 2.2.2 SEM and TEM analysis

Samples micrographs were obtained with a field emission Scanning Electron Microscopy (SEM) apparatus (JSM-6700F, JEOL) instrument operating at 3 kV. Some of the nanocomposites section were cut from the solid samples by a sledge microtome. These slices were etched before the observation by SEM following a procedure already described in Guadagno et al [28, 29]. The transmission electron microscopy (TEM) characterization was performed on a JEOL 2010 LaB<sub>6</sub> microscope operating at 200

kV. Nanopowder was dispersed (in ethanol) by ultrasonic waves for 30 min. The obtained suspension was dropped on a copper grid (Holey carbon).

### 2.2.3 Mechanical and electrical analysis

In order to investigate the mechanical and piezoresistive behavior of the nanocomposites, axial and flexural response strength measurements were performed in agreement with ASTM standards D638 and D790, respectively [30, 31], using a Dual Column Tabletop Testing Systems (INSTRON, series 5967) set with a cross head speed of 1 mm/min for both loading and unloading. In particular, for the flexural tests a configuration of a three point-bending mode is adopted. The corresponding force was measured by the machine load cell and converted to axial stress ( $\sigma$ ), whereas mechanical strain ( $\epsilon$ ) was calculated as the machine crosshead displacement normalized by the gage length of the test specimen. In order to exclude possible slipping during the displacement, the local deformation was detected by means of a conventional strain gage (RS 5 mm Wire Lead Strain, gauge factor 2.1) bonded to one side of the specimen and having a gauge resistance of 120  $\Omega$  constantly measured with a precision multimeter HP 34401A. Copper electrodes were fixed on the sample surface using silver paint (Silver Conductive Paint, resistivity of 0.001  $\Omega$  cm) thus ensuring a good ohmic contact between the parts for the measurement of the resistance,  $R$ , of the samples using the two-probe method with a Multimeter Keithley 6517A configured in the double function of voltage generator and ammeter. This measurement method, although simple, has successfully been applied in literature for resistance measurements in presence of tensile test [16, 32]. Contact resistance was neglected since the measured electrical resistance for all specimens was in the order of several k $\Omega$ . The same electrodes were used for the impedance spectroscopy (IS) analysis performed with a precision LCR meter (model QuadTech 7600). The overall test setup and the geometrical features of the investigated specimens are reported in figure 1.

## 3. Result and discussions

### 3.1 Preliminary morphological and electrical characterization

In order to fully investigate the characteristics of the employed nanofillers a structural and morphological characterization is carried out on them by means of various type of analysis. The Raman spectra collected for MWCNT is shown in figure 2. Raman spectroscopy of CNT may provide information on the degree of structural ordering and then on the bonding states of carbons in the nanotube structures. For sake of clarity and completeness of the present work, the main observed features already presented in Guadagno

et al. are here briefly summarized [33]. In agreement with the Raman spectra for carbonaceous material, it is worth to note two strong bands, the D mode ( $1350\text{ cm}^{-1}$ ) and the tangential stretching G mode ( $1586\text{ cm}^{-1}$ ) and two weak bands, the G' band (overtone of D mode) at  $2700\text{ cm}^{-1}$  and the 2LO band (overtone of LO mode) at  $2900\text{ cm}^{-1}$ . In particular, the band at  $\sim 1350\text{ cm}^{-1}$  is known as the disorder-induced D band and it is observable when defects are present in the carbon aromatic structure. Therefore, this band together with the G'-band can be used for material characterization to probe and monitor structural modifications of the nanotube sidewalls caused by the introduction of defects and the attachment of different chemical species [34]. The G-band exhibits a weakly asymmetric characteristic line shape, with a peak appearing close to the graphite frequency ( $1582\text{ cm}^{-1}$ ). The intensity and characteristics of this band provide information on the order of graphitic layers in the carbon nanostructured forms [35-37]. In particular, a high ratio R of intensities of the D and G bands ( $R = I_D/I_G = 1.19$ , in our case) indicates a high quantity of structural defects. A detailed analysis of the morphological parameters of the CNT has been carried out by high resolution transmission electron microscopy (HR-TEM). The MWCNT are characterized by an outer diameter ranging from 10 to 30 nm whereas their length is from hundreds to some thousands of nm. Instead, the number of shells varies from 4 to 20 in most nanotubes. The strain sensing properties of the nanocomposites depend on the intrinsic response of the constituent materials (i.e., resin and MWCNT) and on their mutual interactions which are governed by the interfacial properties. The distribution of the filler within the resin which determines the electrical percolation network and the formation of conductive junctions (i.e., CJ) due to the tunneling effect between neighbor tubes, can be highlighted by means of scanning electron microscopy (SEM) of a fractured surface of a nanocomposite, as shown in figure 3. In particular, the piezoresistivity behavior observed in the strain sensors based on CNT/polymer nanocomposites is attributable to relevant changes in the electrical network, e.g. loss of contact among CNT [38], variation in the tunneling resistance due to the rearrangement of neighboring CNT [4, 39] and intrinsic piezoresistivity of fillers due to their deformation [7, 40]. As a consequence, there is in general, a new arrangement of the filler that results in small but experimentally detectable changes in the electrical properties. A preliminary electrical characterization focused on the DC volume conductivity of the composites is carried out without applying any strain (zero load) in order to identify a suitable filler concentration to be considered for testing under axial tension and flexural stress. Therefore in figure 4 the electrical conductivity ( $\sigma$ ) as function of the amount of MWCNT ( $\nu$ ) is reported. As expected by the percolation theory, the conductivity depends on the filler loading in agreement with a scaling law of the type:

$$\sigma = \sigma_0(v - v_c)^t \quad (1)$$

where  $v_c$  is the amount corresponding to percolation threshold,  $\sigma_0$  is the filler conductivity and  $t$  an exponent depending on the system dimensionality [41]. In particular, conductive paths are formed in the composite when the CNT amount (i.e.  $v$ ) increases over a threshold value (EPT, i.e.  $v_c$ ) thus leading the material to convert from an insulator to a conductor behavior. It is worth to note that, as the concentration of the conductive fillers approaches the EPT, which is in the range [0.1-0.3 wt%], an abrupt increase in the electrical conductivity of the composites, compared with the few pS/m characterizing the pure resin, can be observed. A value of about 0.29 S/m is achieved at the highest filler loading (i.e. 1 wt%). It is worth noting that the values of EPT and electrical conductivity beyond the EPT greatly depend on the chemical nature of the hosting matrix, as well as on the manufacturing methods. As an instance, the same MWCNTs, embedded in resins characterized by very low values of viscosity, are able to give lowest EPT values [42]. This different behaviour is most likely due to a strong influence of the viscosity on the nanofiller dispersion state. The value of the exponent  $t$  (i.e. 2.2) of the percolation law, obtained as the slope of the linear interpolation in the inset of figure 4, is found to agree with universal values typically reported in literature. The sensitivity of the composites reinforced with carbon-base filler, as reported in different literature studies [3, 43, 44], is low when the composite acts as an insulator (below the EPT) and decreases significantly as the weight loading of CNT increases in the high conductivity region. Therefore, the region around the EPT is the most suitable for sensor applications [45-47]. Hence, in this paper the mechanical and piezoresistive tensile response of an epoxy resin suitable for the realization of structural aeronautic components and reinforced with 0.3 %wt of multi-walled carbon nanotubes (MWCNT) was investigated when specimens are subjected to a low number of fatigue cycles in axial and flexural mode. Such specific filler concentration has been chosen since it is a first concentration above the EPT and because in aeronautical composites a good electrical should be ensured. Furthermore, in order to explore the frequency response of the composite, impedance spectroscopy (IS) measurements are performed in the range [10Hz -1MHz] without applying any strain (zero load). Figure 5 shows the plot of magnitude of the overall impedance of material (in  $\Omega$ ) and in the inset the relative phase angle (in degree) and real part of the dielectric permittivity (i.e.  $\epsilon_r$ ) respectively, as a function of the frequency. Such analysis allows to identify the critical frequency  $f_c$  at which the electrical properties change from a frequency-independent to a dispersive (frequency-dependent) behavior [48, 49]. In fact, it is interesting to note that up to 100 KHz the electrical behavior exhibited by the composite is of resistive type since the impedance is almost

constant and a phase about zero as for a resistor. Beyond this critical frequency, the capacitive effects mainly due to the insulating resin become dominant and the impedance varies with the frequency (i.e.  $f$ ) following a trend described by  $|Z| \sim 1/f$  whereas the phase  $\Phi$  deviates from the null value to evolve, at higher frequencies, towards  $-90^\circ$  as for a typical insulating material equivalent from an electrical point of view to a capacitor. Finally, the variations of the real part of the dielectric permittivity vs. frequency can be ascribed to the presence of free dipolar functional groups (mainly of type C-OH or sometimes N-H as reaction product) and more significantly to interfacial polarization attributable to the presence of conducting impurities. At low frequency the system shows the highest value and, as the frequency increases, the permittivity progressively decreases because both mechanisms become negligible.

### 3.2 DC Piezoresistive characterization

#### 3.2.1 Tensile stress

Figure 6a shows the mechanical and piezoresistive performances of the epoxy-based composites reinforced with 0.3 wt% of MWCNT when loaded in axial tension up to failure. In particular, the results concern the normalized change of electrical resistance  $\Delta R/R_0$  (right vertical axis), where  $R_0$  is the steady-state electrical resistance of the material without applying any strain (i.e.  $\epsilon=0$ ) and  $\Delta R=R-R_0$  is the instantaneous change in  $R$ , plotted against the axial strain ( $\epsilon$ ). The mechanical loading (i.e.  $\sigma$ ) is also plotted on the left vertical axis. A direct relationship between the two plotted parameters can be observed. First of all, it is essential to identify the different operating regions such as the elastic one corresponding at lower strain levels ( $\epsilon$  up to 2% with respect the rest position) which is followed by the plastic zone for higher loadings that gradually lead to the failure of the sample. In fact, around at the 3.5% of strain we observe a cracking that discontinues the electrical measurements and leads to the specimen collapse, as shown in figure 6a. Therefore, the levels of strain in the subsequent experimental tests will be kept below this indicative critical value. In the first region corresponding to the elastic response of the material a linear mechanical behavior correlates with a linear piezoresistive curve as evident from the tangent plotted at the origin that coincide with the linear fit of such curves based on the first measured data points. Then, the  $\Delta R/R_0$  curve becomes nonlinear with an evident abrupt change most likely due to the occurrence of the first nano-crackings within the structure. The sensitivity of a piezoresistive sensor, that is desirable to be as high as possible for practical applications, can be quantified in terms of gauge factor, a dimensionless parameter defined as the relative change in electrical resistance due to an applied strain

(i.e.  $G.F.= \Delta R/\epsilon R_0$ ). The value obtained of 0.43 is derived as the slope of the interpolating line of  $\Delta R/R_0$  curve of experimental data that lie in the elastic region. The increase of the overall resistance of the sample with increasing tensile stress agrees with the assumption that in a conductor-filled polymer the main electrical conduction mechanism occurs via "tunneling effect" which requires that the filler particles must be sufficiently close (at the so-called "tunneling distance") to each other to allow the electron flow [49, 50]. As a consequence of the imposed tensile strain, it is reasonable that the tunneling resistance could vary between neighboring CNT due to the enlargement of inter-tube distance and/or a decreasing of the electrical contact areas. Both phenomena lead to an increase of the resistance exhibited by the sample. In order to investigate the reversibility and stability of sensor properties of the nanocomposites, specimens were subjected to tensile loading cycles based on increases/decreases of some selected level strains. As shown in figure 6b, increasing strain per cycle was applied (i.e. 0.83%, 1.65% and 2.42%), and the temporal behavior of the piezoresistive response was monitored. The resistive behavior of the sample is regular since, for the same value of the strain in each cycle, the variation of electrical resistance show comparable values of the  $\Delta R/R_0$  ratio. It is worth noting that, when the crosshead returns to the initial position, for lower levels of strain that fall in the elastic regime (i.e.  $\epsilon=0.83\%$  and  $\epsilon=1.65\%$ ),  $\Delta R/R_0$  returns to zero after each loading cycle, indicating that significant permanent deformation or irreversible damage has not occurred in the composite. Otherwise, for higher value of tensile strain (i.e.  $\epsilon=2.42\%$ ), when the deformation exceed the elastic response of the sample evolving toward the plastic one, it can be noted a change in resistance value that start to become irreversible for unloaded sample (i.e.  $\sigma=0$ ). In particular, the presence of a residual resistance appears due to some damage in the sensor most likely as a result of a permanent and irreversible phenomena (yielding) in electrical percolating network associated to morphological rearrangement of the CNT dispersed in the polymer resin and to the fatigue and plastic deformation of the latter. Therefore, in plastic regime the sensor system may allow the detection of possible damages in the monitored part [16, 44, 51].

### 3.2.2 Flexural stress

The change of electrical resistance was also correlated to bending deformations. Other literature studies report experiments performed in the 4-points-bending mode on thermoplastic polymers and rubbers [47, 52]. Here, the flexural stress-strain curves are obtained from three point bend test of the samples. The obtained results are shown in figure 7a. In order to prevent possible discrepancies during the

displacement, the flexural strain was detected by means of a conventional strain gauge. In table 1 the experimentally detected values are also compared to those evaluated from the following relation:

$$\varepsilon_{flexural} = \frac{6Dt}{L^2} \quad (2)$$

where  $D$  is the maximum deflection of the center of the sample (mm),  $t$  is the thickness of the sample (mm) and  $L$  is the support span (mm). From the analysis of the data in Table 1 it can be noted that the theoretical values are always lower than those achieved by measurement. Differently from the piezoresistive behavior observed in tensile test, the normalized change of electrical resistance  $\Delta R/R_0$  vs. strain measured in such mode is nonlinear in the whole strain range and follows an exponential law, as reported in figure 7a. Also under flexural stress condition, different cycles in z-displacement with several level of strain were applied to the specimens. The mechanical behavior and change of electrical resistance as function of time were measured and correlated to strain, as show in figure 7b. It is evident that the electrical resistance changes vary with the intensity of strain and that the maximum value achieved for each level of deformation is maintained for different cycles. Moreover, the resistance resumes its initial value under an applied strain up to 2.06% which, as indicted in figure 7a, falls in the elastic regime. This reproducible resistive response during the mechanical cycles indicates that no ruptures or permanent deformation has occurred in the material structure. The different behaviors observed for the two types (tensile and flexural) of imposed stresses may be justified by considering Saint Venant's theory and Navier's formulas, under the hypothesis of plane and small deformations [53, 54]. In presence of tensile stress, i.e. the application of a traction force normal to the surface, the material reacts with a simple stretching in the direction of the force. This stretching is uniform in the entire cross-section of the load application. As a consequence, the percolating network moves rigidly with the force and the electrical response appear linear. Instead, under flexural stress, the behavior may be attributed to an inflection giving a curvature according to an arc of circumference generated by the bending moment (i.e.  $M$ ). As a consequence, in this case the electrical response of the material is influenced by a combination of two coexisting dynamic effects. In fact, following this inflection (those above the neutral plane, i.e. np) parts of the specimen and in particular that of the resin, which acts as an insulating spacer between the conductive particles, will shorten due to the action of the internal compressive stresses (i.e.  $\sigma_c$ ) and other (those below the neutral plane) will lengthen due to internal tensile stresses (i.e.  $\sigma_t$ ), as shown in figure 8. With the gradual increment of specimen curvature, due the increasing strain values, the elongation of

resin in the convex part will predominate over the compression of the same in the concave part. As a result, the tunneling resistance between nanotubes, particularly sensitive to distance variations, affects more significantly the electrical response of the material thus originating the exponential dependence of the  $\Delta R/R_0$  vs. strain.

### 3.3 AC characterization

#### 3.3.1 Tensile stress

The sensitivity of the composites evaluated with DC measurements has been also compared with that obtained by impedance analysis (see figure 9), in order to evaluate a possible contribution of the dielectric properties on sensing performances. In fact, from the preliminary AC investigation illustrated in figure 5, the impedance of the sample, starting from the frequency of 100 kHz was found to be dispersive (frequency dependent) due to capacitive effects that start to become dominant over those associated to the conduction, thereby influencing the macroscopic AC properties of the composites. The strain sensitivity of the composites under tensile loads in AC was investigated in terms of gauge factor (i.e. G.F.) defined as the normalized variation of the electrical impedance  $\Delta Z/Z_0$  as function of the axial strain (i.e.  $\epsilon$ ) where  $\Delta Z$  and  $Z_0$  are the instantaneous change in the electrical impedance and its initial value before mechanical loading (i.e.  $\sigma=0$ ), respectively. It is possible to note that the G.F. improves significantly as the frequency increases and in particular the most favorable value is observed at 1MHz where G.F. is 0.60, about 40% higher than that estimated in DC. This improvement in the sensitivity may be attributed to a synergy between the capacitive and resistive effects that coexist in a composite system with an insulating matrix filled with a conductive phase and that can magnify the response of the sensor [55]. In fact, the AC properties of the polymer/carbon based composites can be analyzed by using a single-time-constant equivalent circuit model (i.e. STC circuit) whose overall impedance is given by the parallel combination of a resistor (i.e.  $R_p$ ) and capacitor (i.e.  $C_p$ ) as shown in figure 10. The relations between the impedance and the electrical parameters of the equivalent circuit are:

$$|Z| = \frac{R_p}{\sqrt{1 + \omega^2 R_p^2 C_p^2}}, \quad \varphi = \arctan(\omega R_p C_p) \quad (3)$$

where, at first approximation,  $R_p$  takes into account the conduction via the CNT-particles percolative network (i.e. tunneling resistance,  $R_{\text{tun}}$ ) and  $C_p$  takes into account the small but diffuse coupling capacitances between the neighboring CNT separated by a thin insulating film and mainly the

“background” dielectric behavior of the resin (i.e.  $C_{res}$ ) which as a first approximation can be considered as that of a parallel-plate capacitor [49, 56, 57].

In particular these electrical effects can be quantified according to the following expressions:

$$R_{tun} = \frac{h^2 d}{S e^2 \sqrt{2 m_e \lambda}} \exp\left(\frac{4 \pi d}{h} \sqrt{2 m_e \lambda}\right); \quad C_{res} \quad (4)$$

$$= \epsilon_0 \cdot \epsilon_{res} \cdot \frac{A}{d_s}$$

where  $h$  is the Plank’s constant,  $e$  is the electron charge,  $m_e$  is the mass of electron,  $\lambda$  is the height of barrier,  $d$  and  $S$  are respectively the distance between conductive particles and the area involved in the tunneling phenomena approximated as the cross-sectional area of the CNT,  $\epsilon_0$  and  $\epsilon_{res}$  are respectively the permittivity of free space and that of the neat resin, while  $A$  and  $d_s$  are the area of plates and their separation. The tunneling resistance increases with the particle separation up to of a cut-off distance (about 2 nm); unlikely, the capacitance, decreases as the particle distance increases. The changes in the values of resistances and capacitances of the sensor under different level of strain are analyzed at the frequency of 1MHZ and the results are shown in figure 11. As expected and experimentally observed also in other literature study [21] the distances between the conductive CNT-particles increase with the increment of strains and, as a consequence,  $R_p$  increases and  $C_p$  decreases. Figure 12a shows the mechanical and AC piezoresistive response of the nanocomposites measured at operating frequency of 1MHz when strain that falls in the elastic regime of the material is applied in order to evaluate the gauge factor. In particular, the results concern the normalized change of electrical impedance  $\Delta Z/Z_0$  (right vertical axis), and that of mechanical loading (i.e.  $\sigma$ , left vertical axis) plotted against the axial strain ( $\epsilon$ ). It is possible to observe that  $\Delta Z/Z_0$  increases linearly as a function of the tensile strain with  $\Delta Z/Z_0 \sim k\epsilon$  where  $k$ , coincident with the G.F. (i.e. 0.60), is the slope of the interpolating line of the  $\Delta Z/Z_0$  curve and therefore representative of the piezoresistive tensile behavior of the composite. In order to analyze the dynamic durability in terms of mechanical integrity and electrical functionality, the endurance of strain sensors to subsequent stretching/releasing cycles at different level of strains is tested with AC measurements and the results are compared to the values obtained with DC investigations. In particular, figure 12b shows this comparison for the average values of both the maximum resistance and impedance change ratios measured at each level of strain during the different cycles. An evident increment appears if the strain is evaluated in terms of changes of impedance rather than that of resistance variations. In fact,

regardless the level of strain, the sensor exhibits higher strain sensitivity in AC than in DC due to the additional contributions of the capacitive elements.

### 3.3.2 Flexural stress

Figure 13 shows the experimental results concerning the piezoresistive response of the material, in terms of impedance changing ratio, when subjected to bending loads, evaluated at different operating frequency. From the plots it is evident that the electrical response follows exponentially the mechanical deformation consistently with the results observed in DC. Given the nonlinearity of the curves, it is technically impossible to extrapolate a sensitivity index from such measures. After all, it would be meaningless because sensor nonlinearity could make the calibration process particularly difficult and complex. However, it is worth noting as shown in figure 13, how the concavity of the curve tends to become less pronounced with increasing frequency. Particularly interesting is the measurements carried out at the frequency of 1 MHz identified in the previous analysis. In fact, at this frequency the behavior of the composite follows an almost linear trend with the mechanical stress. Therefore, in figure 14a the flexural stress (i.e.  $\sigma$ , left vertical axis) and normalized change of electrical impedance (i.e.  $\Delta Z/Z_0$ , right vertical axis) as function of the strain ( $\epsilon$ ) are shown. In this case, it is possible to fit the curves of the experimental data with a linear regression whose slope provides the G.F. of sensor for which a value of 1.28 is obtained. Moreover, following the same procedure described in the previous sections to verify the dynamic durability of the sensor, AC measurement are carried out on the specimens and the results are reported in figure 14b. The electrical response of the sample is stable since the impedance variations, at the same value of the strain, exhibits comparable values (%) in the ratio  $\Delta Z/Z_0$ . Furthermore, the electrical response follows linearly the mechanical deformation, both during the loading and the unloading phases. Since the deformation loads are limited in the elastic regime of the material (about 2%)  $\Delta Z/Z_0$  returns to the initial value after each loading cycles thus indicating that the applied strain induces reversible variations in the nanotube network configuration. Finally, as reported in figure 15, the resistance and impedance change ratios (i.e.  $\Delta R/R_0$  and  $\Delta Z/Z_0$ , respectively) are compared for each level of strain in terms of average of the maximum value measured in each cycle. It is interesting to note that in flexural mode there is a remarkable difference, greater than two order of magnitude, if the strain is detected in terms of variation of impedance rather than resistance. In fact, if the small strain of 0.7% applied to the sample induces a resistance change ratio of only 0.2%, the same strain leads to a variation

of impedance change ratio of 1.1%. The sensitivity vs. strain is about 108 times greater for the measurements performed in the AC with respect to that in DC.

#### 4. Conclusions

The piezoresistive behavior of an structural resin, particularly indicated for aircraft applications and reinforced with a specific amount of MWCNT, was investigated with DC and AC measurements when the specimens are subjected to a low number of cycles and different levels of strain loaded in both axial tension and flexural mode. The piezoresistive properties can be mainly attributed to the re-arrangement of conductive percolating network formed by MWCNT induced by the deformation of the material due to the applied stresses. It is found that the sensitivity of sensor, quantified in terms of gauge factor increases with the increases of the frequency. The AC measurements are more effective than those in DC, due to the combined action of the resistances and capacitances that determine the overall electrical response of the material. At an optimal operating frequency of 1MHz there is an improvement of the sensitivity to the strain of more than two orders of magnitude compared to the results of the DC characterization. Furthermore, dynamic durability of the sensor, which is a fundamental requirement especially for structural aircraft monitoring applications, was tested during stretching/releasing cycles. The nanocomposites showed high sensibility, reliability and reversible response. Future works will attempt to analyze composites subjected to cycling stresses of long duration and systems with different concentrations and type of fillers such as carbon fibers or graphene sheets in order to support the selection of functional nanomaterials with improved and tailored piezoresistive properties.

#### Acknowledgments

This work was supported by Regional funds “Assegni di Ricerca Regione Campania - ASSEGNIREG” (CUP: D42I15000270006) and performed within the European Union's Seventh Framework Programme for research, technological development and demonstration under Grant Agreement no 313978.

#### References

- [1] Kang I, Schulz MJ, Kim JH, Shanov V, Shi D. A carbon nanotube strain sensor for structural health monitoring. *Smart Mater Struct* 2006;15:737-748.

- [2] Topolov VYu, Bowen CR, Bisegna P. New aspect-ratio effect in three-component composites for piezoelectric sensor, hydrophone and energy-harvesting applications. *Sensor Actuat A-Phys* 2015;229:94-103.
- [3] Kang I, Heung YY, Kim JH, Lee JW, Gollapudi R, Subramaniam S, et al. Introduction to carbon nanotube and nanofiber smart materials. *Compos Part B-Eng* 2006; 37:382-394.
- [4] De Vivo B, Lamberti P, Spinelli G, Tucci V, Vertuccio L, Vittoria V. Simulation and experimental characterization of polymer/carbon nanotubes composites for strain sensor applications. *J Appl Phys* 2014;116:054307 -14.
- [5] Dargahi J. A piezoelectric tactile sensor with three sensing elements for robotic, endoscopic and prosthetic applications. *Sensor Actuat A-Phys* 2000;80:23-30.
- [6] Tomblor TW, Zhou C, Alexseyev L, Kong J, Dai H, Liu L, et al. Reversible electromechanical characteristics of carbon nanotubes under local-probe manipulation. *Nature* 2000;405:769-772.
- [7] Yang L, Han J. Electronic Structure of Deformed Carbon Nanotubes. *Phys Rev Lett* 2000; 85:154-157.
- [8] Song X, Liu S, Gan Z, Lv Q, Cao H, Yan H. Controllable fabrication of carbon nanotube-polymerhybrid thin film for strain sensing. *Microelectron Eng* 2009;86:2330-2333.
- [9] Häntzsche E, Matthes A, Nocke A, Cherif Ch. Characteristics of carbon fiber based strain sensors for structural-health monitoring of textile-reinforced thermoplastic composites depending on the textile technological integration process. *Sensor Actuat A-Phys* 2013; 203: 189-203.
- [10] Williams JC, Starke AE Jr. Progress in structural materials for aerospace systems. *Acta Mater* 2003;51:5775-5799.
- [11] Kawakami H, Feraboli P. Lightning strike damage resistance and tolerance of scarf-repaired mesh-protected carbon fiber composites. *Compos Part A-Appl S* 2011;42:1247-1262.
- [12] Larsson A. The interaction between a lightning flash and an aircraft in flight. *C R Physique* 2002;3:1423-1444.
- [13] Park S, Shin HH, Yun CB. Wireless impedance sensor nodes for functions of structural damage identification and sensor self-diagnosis. *Smart Mater Struct* 2009;18:055001-(11pp).
- [14] Ning Hu, Karube Y, Arai M, Watanabe T, Yan C, Li Y, et al. Investigation on sensitivity of a polymer/carbon nanotube composite strain sensor. *Carbon* 2010; 48:680-687.

- [15] Serra N, Maeder T, Ryser P. Piezoresistive effect in epoxy–graphite composites. *Sensor Actuat A-Phys* 2012;186:198–202. DOI:10.1016/j.sna.2012.04.025
- [16] Ku-Herrera JJ, Aviles F. Cyclic tension and compression piezoresistivity of carbon nanotube/vinyl ester composites in the elastic and plastic regimes. *Carbon* 2012;50:2592-2598.
- [17] Amjadi M, Kyung KU, Park I, Sitti M. Stretchable, skin-mountable, and wearable strain sensors and their potential applications: A review. *Adv Funct Mater* 2016;26:1678-1698.
- [18] Gaiser P, Binz J, Gompf B, Berrier A, Dressel M. Tuning the dielectric properties of metallic-nanoparticle/elastomer composites by strain. *Nanoscale* 2015;7:4566-4571.
- [19] Loh KJ, Kim J, Lynch JP. Self-sensing and power harvesting carbon nanotube-composites based on piezoelectric polymers. 4th International Conference on Bridge Maintenance, Safety and Management. Seoul (Korea): CRC Press; Taylor & Francis Group, 2008; p. 3329-3336.
- [20] Mei H, Zhang C, Wang R, Feng J, Zhang T. Impedance characteristics of surface pressure-sensitive carbon black/silicone rubber composites. *Sensor Actuat A-Phys* 2015; 233:118-124.
- [21] Wang SL, Wang P, Ding TH. Piezoresistivity of silicone-rubber/carbon black composites excited by Ac electrical field. *J Appl Polym Sci* 2009;113:337–341.
- [22] Mohanraj GT, Chaki TK, Chakraborty A, Khashtgir D. Effect of some service conditions on the electrical resistivity of conductive styrene–butadiene rubber–carbon black composites. *J Appl Polym Sci* 2004;82:2179–2188.
- [23] Brosseau C, NDong W, Mdharhri A. Influence of uniaxial tension on the microwave absorption properties of filled polymers. *J Appl Phys* 2008; 104:074907-1 074907-7.
- [24] Guadagno L, Raimondo M, Vittoria V, Vertuccio L, Naddeo C, Lamberti P, et al. Epoxy resin with low humidity content. European Patent Application EP2873682 (A1), 2015. Also published as: ITTO20130926 (A1) - Resina epossidica con basso tenore di umidità.
- [25] Nobile MR, Raimondo M, Lafdi K, Fierro A, Rosolia S, Guadagno L. Relationships between nano filler morphology and viscoelastic properties in CNF/epoxy resins. *Polym. Compos.* 2015;36:1152-1160.
- [26] Guadagno L, Raimondo M, Vittoria V, Vertuccio L, Naddeo C, Russo S, et al. Development of epoxy mixtures for application in aeronautics and aerospace. *RSC Adv* 2014;4:15474 – 15488.

- [27] Raimondo M, Russo S, Guadagno L, Longo P, Chirico S, Mariconda A, et al. Effect of incorporation of POSS compounds and phosphorous hardeners on thermal and fire resistance of nanofilled aeronautic resins. *RSC Adv* 2015;5:10974-10986.
- [28] Guadagno L, Raimondo M, Vertuccio L, Mauro M, Guerra G, Lafdi K, et al. Optimization of graphene-based materials outperforming host matrices. *RSC Adv* 2015;5:36969–36978.
- [29] Guadagno L, Raimondo M, Vittoria V, Vertuccio L, Lafdi K, De Vivo B, et al. The role of carbon nanofiber defects on the electrical and mechanical properties of CNF-based resins. *Nanotechnology* 2013; 24:305704 (pp.10).
- [30] ASTM D638. Standard Test Method for Tensile Properties of Plastics, West Conshohocken, PA: ASTM International; 2010.
- [31] ASTM D790. Standard Test Methods for Flexural Properties of Unreinforced and Reinforced Plastics and Electrical Insulating; 2010.
- [32] Oliva-Avilés AI, Avilés F, Sosa V. Electrical and piezoresistive properties of multi-walled carbon nanotube/polymer composite films aligned by an electric field. *Carbon* 2011;49:2989-2997.
- [33] Guadagno L, De Vivo B, Di Bartolomeo A, Lamberti P, Sorrentino A, Tucci V, et al. Effect of functionalization on the thermo-mechanical and electrical behavior of multi-wall carbon nanotube/epoxy composites. *Carbon* 2011;49:1919-1930.
- [34] Dresselhaus MS, Dresselhaus G, Saito R, Jorio A. Raman spectroscopy of carbon nanotubes. *Phys Rep* 2005,409:47-99.
- [35] Liu Y, Vander Wal RL, Khabashesku VN. Functionalization of carbon nano-onions by direct fluorination. *Chem Mater* 2007;19:778-786.
- [36] Osswald S, Havel M, Gogotsi Y. Monitoring oxidation of multiwalled carbon nanotubes by Raman spectroscopy. *J Raman Spectrosc* 2007;28:728-736.
- [37] Costa S, Borowiak-Palen E, Kruszynska M, Bachmatiuk A, Kalenczuk RJ. Characterization of carbon nanotubes by Raman spectroscopy. *Mater Sci. (Poland)*. 2008 ;26:433-441.
- [38] Park M, Kim H, Youngblood JP. Strain-dependent electrical resistance of multi-walled carbon nanotube/polymer composite films. *Nanotechnology* 2008;19:055705(7pp).
- [39] Wichmann MHG, Buschhorn ST, Gehrman J, Schulte K. Piezoresistive response of epoxy composites with carbon nanoparticles under tensile load. *Phys Rev B* 2009;80:245437-1; 245437-8.

- [40] Yang L, Anantram MP, Han J, Lu JP, Band-gap change of carbon nanotubes: Effect of small uniaxial and torsional strain. *Phys Rev B* 1999;60:13874-13878.
- [41] Nan CW, Shen Y, Ma J. Physical Properties of Composites Near Percolation. *Annu Rev Mater Sci.* 2010; 40:131-151.
- [42] Kotsilkova R, Ivanov, Bychanok D, Paddubskaya A, Demidenko M, Macutkevic J, et al. Effects of Sonochemical Modification of Carbon Nanotubes on Electrical and Electromagnetic Shielding Properties of Epoxy Composites. *Compos Sci Technol* 2015;106:85-92
- [43] Pham GT, Park YB, Liang Z, Zhang C, Wang B. Processing and modeling of conductive thermoplastic/carbon nanotube films for strain sensing. *Compos Part B-Eng* 2008;39:209-216.
- [44] Vertuccio L, Vittoria V, Guadagno L, De Santis F. Strain and damage monitoring in carbon-nanotube-based composite under cyclic strain. *Compos Part A Appl Sci Manuf* 2015;71:9-16.
- [45] Ferreira A, Rocha JG, Ansòn-Casaos A, Martínez MT, Vaz F, Lanceros-Mendez S. Electromechanical performance of poly(vinylidene fluoride)/carbon nanotube composites for strain sensor applications. *Sensor Actuat A-Phys* 2012;178:10-16.
- [46] Simoes R, Silva J, Vaia R, Sencadas V, Costa P, Gomes J, et al. Low percolation transitions in carbon nanotube networks dispersed in a polymer matrix: dielectric properties, simulations and experiments. *Nanotechnology* 2009;20:035703(p8).
- [47] Paleo-Vieto AJ, van Hattum FWJ, Pereira J, Rocha J G, Silva J, Sencadas V, et al. The piezoresistive effect in polypropylene-carbon nanofibre composites obtained by shear extrusion. *Smart Materials and Structures* 2010;19:065013(p7).
- [48] Connor MT, Roy S, Ezquerra TA, Balta-Calleja F J. Broadband AC conductivity of conductor-polymer composites. *Phys Rev B: Condens Matter Mater Phys* 1998;57:2286-2294.
- [49] De Vivo B, Lamberti P, Spinelli G, Tucci V. Numerical Investigation on the Influence Factors of the Electrical Properties of Carbon Nano Tubes-filled Composites. *J Appl Phys* 2013;113: 244301-12.
- [50] Thostenson ET, Ren Z, Chou TW. Advances in the science and technology of carbon nanotubes and their composites: a review. *Compos Sci Technol* 2001;61:1899–1912.
- [51] Böger L, Wichmann MH, Meyer LO, Schulte K. Load and health monitoring in glass fibre reinforced composites with an electrically conductive nanocomposite epoxy matrix. *Compos Sci Technol* 2008; 68:1886-1894.

- [52] Costa P, Ferreira A, Sencadas V, Viana JC, Lanceros-Méndez S. Electro-mechanical properties of triblock copolymer styrene-butadiene-styrene/carbon nanotube composites for large deformation sensor applications. *Sensor Actuat A-Phys* 2013; 201:458-467.
- [53] Ascione L. *Elementi di scienza delle costruzioni*. Salerno, Italy: CUES editrice; 2001.
- [54] Di Francesco R. *Introduzione alla meccanica del continuo*. Palermo, Italy: Dario Flaccovio editore; 2012.
- [55] Norman F, Sheppard Jr, Senturia SD. Chemical interpretation of the relaxed permittivity during epoxy resin cure. *Polym. Eng. Sci.* 1986;26:354–357.
- [56] De Vivo B, Lamberti P, Tucci V, Kuzhir PP, Maksimenko SA, Bellucci S. Equivalent electric circuits for the simulation of carbon nanotube-epoxy composites. *IEEE Trans Nanotechn* 2013;12:696-703.
- [57] Li C, Thostenson ET, Chou TW. Dominant role of tunneling resistance in the electrical conductivity of carbon nanotube-based composites. *Appl Phys Lett* 2007;91:223114-3

#### List of Table Captions

**TABLE 1:** Comparison of the flexural strains evaluated from theory and with a strain gauge

#### List of Figure Captions

**FIGURE 1.** Experimental setup and specimen characteristics for piezoresistive characterization in tensile and flexural tests

**FIGURE 2.** Raman spectra of MWCNT.

**FIGURE 3.** High resolution transmission electron microscope images of MWCNT (bottom); SEM images of the fracture of composites with 0.3 wt% loading of MWCNT where possible conductive junction (*CJ*) are identified (down).

**FIGURE 4.** DC volume electrical conductivity ( $\sigma$ ) versus MWCNT weight percentage ( $v$ ). The inset shows the log-log plot of the electrical conductivity as a function of  $(v - v_c)$  with a linear fit.

**FIGURE 5.** Modulus of impedance as function of frequency. Red circle highlights the critical frequency, i.e.  $f_c$ , for such composite. The inset shows the relative phase (degree) and the dielectric permittivity of the specimen vs. frequency.

**Figure 6.** Mechanical behavior (i.e.  $\sigma$ , left vertical axis) and normalized change of electrical resistance (i.e.  $\Delta R/R_0$ , right vertical axis) observed in tensile stress as function of the axial strain ( $\epsilon$ ) and vs. time for cycling tension loading of nanocomposites, in fig. a) and b), respectively.

**FIGURE 7.** Mechanical behavior (i.e.  $\sigma$ , left vertical axis) and normalized change of electrical resistance (i.e.  $\Delta R/R_0$ , right vertical axis) observed in flexural stress as function of the axial strain ( $\epsilon$ ) and vs. time for cycling tension loading of nanocomposites, in fig. a) and b), respectively.

**FIGURE 8.** Dynamic deformation in the case of bending stress (left) and geometrical effect on the CNT morphological electrical network (right).

**FIGURE 9.** Sensitivity vs. frequency of the composite under tensile stress. The markers refer to the average value of the measurements carried out on different specimens. The corresponding error bars are also reported.

**FIGURE 10.** Equivalent circuit for the electrical behavior of a nanocomposite

**FIGURE 11.** Resistance and capacitance variation of the sensor under different level of strain for composites analyzed at  $f=1\text{MHz}$ .

**Figure 12.** a) Sensitivity of the composite under tensile stress evaluated in the elastic range; b) Comparison of the sensitivity of the composite under tensile stress measured in DC and AC domain. The markers refer to the average value of the measurements performed on different specimens. The corresponding error bars are also reported.

**Figure 13.** Behavior of normalized change of electrical impedance versus flexural stress at different operating frequency.

**Figure 14.** Mechanical behavior (i.e.  $\sigma$ , left vertical axis) and normalized change of impedance (i.e.  $\Delta Z/Z_0$ , right vertical axis) measured at the optimal operating frequency of 1MHz in flexural stress as function of the axial strain ( $\epsilon$ ) and vs. time for cycling tension loading of nanocomposites, in fig. a) and b), respectively.

**Figure 15.** Comparison of the sensitivity to strain of the composite evaluated with DC and AC measurements. The markers refer to the average value of the measurements performed on different specimens. The corresponding error bars are also reported.

**TABLE 2:** Comparison of the flexural strains evaluated from theory and with a strain gauge

$\epsilon_{\text{flexural}}$	[%]
Theory	0.29 - 0.58 - 0.87 - 1.16 - 1.46 - 1.75 - 2.04 - 2.33 - 2.63 - 2.92
Strain Gauge	0.34 - 0.69 - 1.04 - 1.38 - 1.73 - 2.07 - 2.42 - 2.76 - 3.11 - 3.45

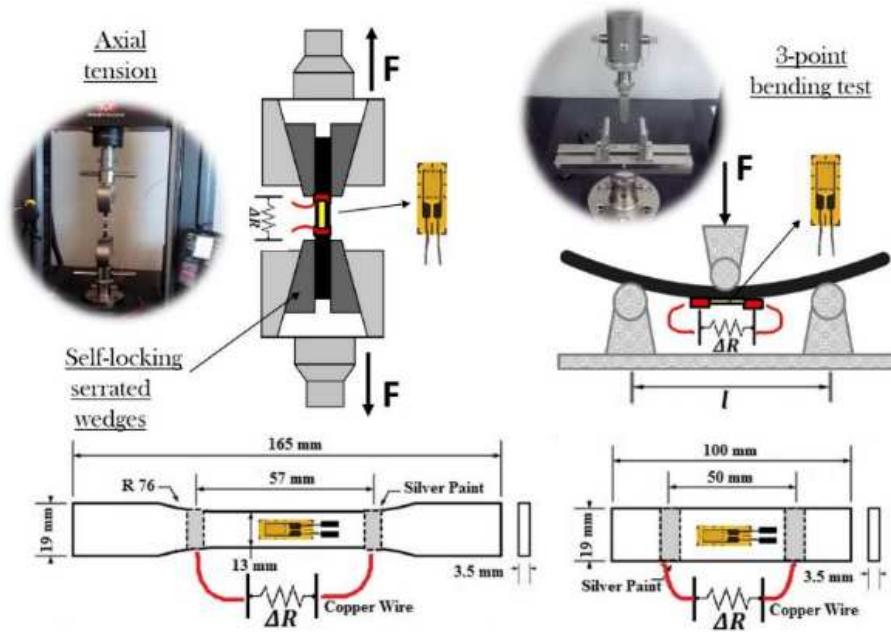


**FIGURE 2.** Experimental setup and specimen characteristics for piezoresistive characterization in tensile and flexural tests

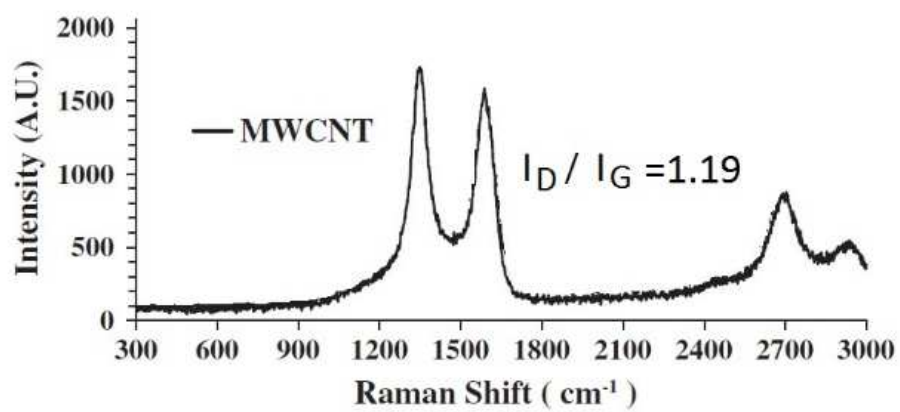
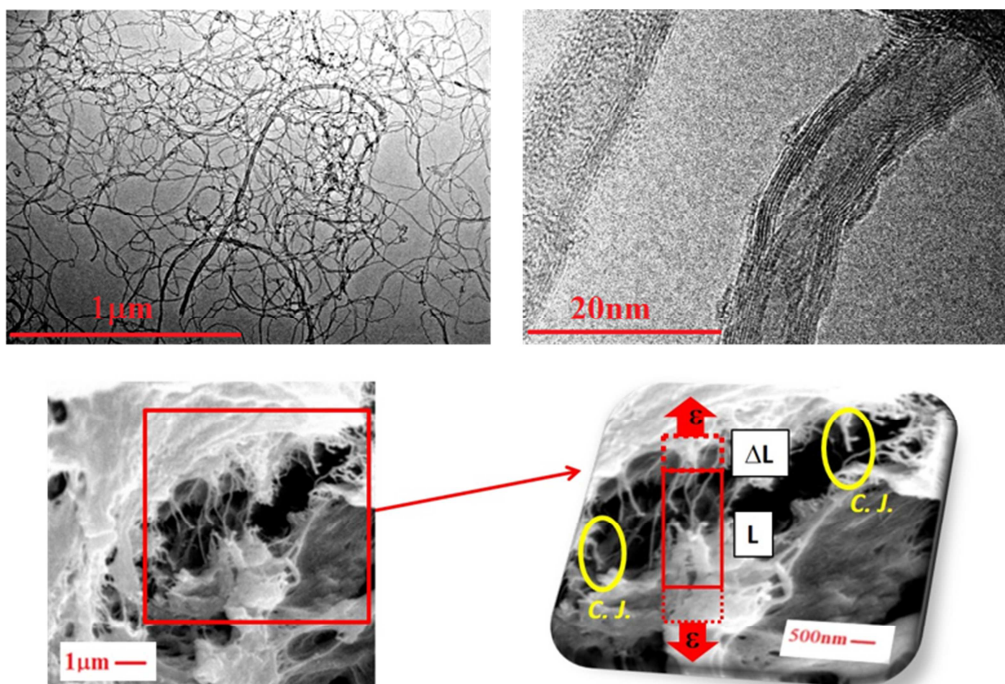
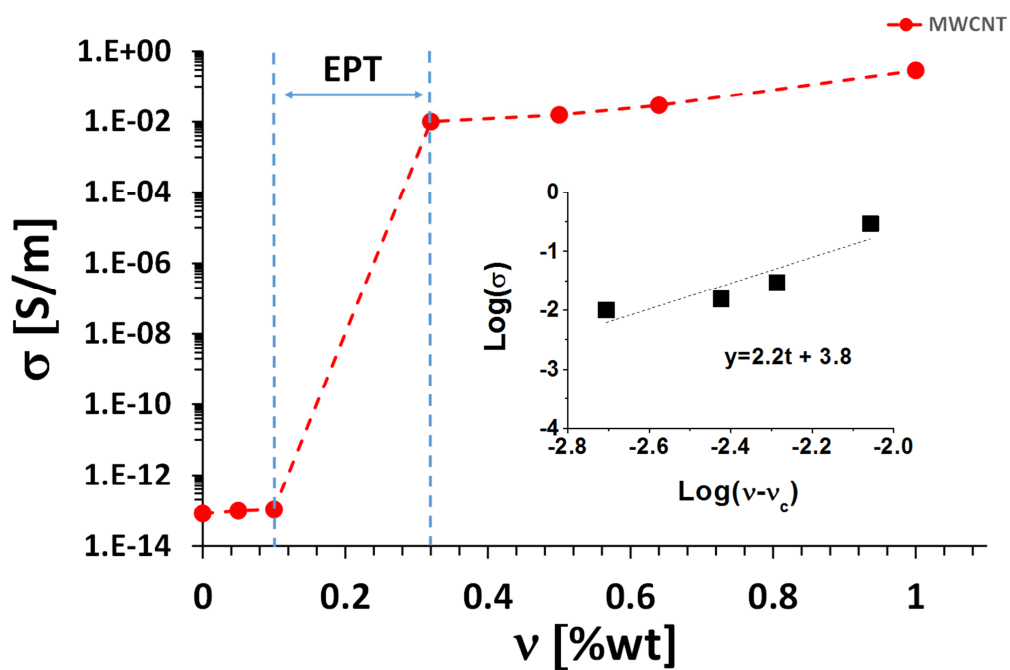


FIGURE 2. Raman spectra of MWCNT.



**FIGURE 3.** High resolution transmission electron microscope images of MWCNT (bottom); SEM images of the fracture of composites with 0.3 wt% loading of MWCNT where possible conductive junction (*CJ*) are identified (down).



**FIGURE 4.** DC volume electrical conductivity ( $\sigma$ ) versus MWCNT weight percentage ( $v$ ). The inset shows the log-log plot of the electrical conductivity as a function of  $(v - v_c)$  with a linear fit.

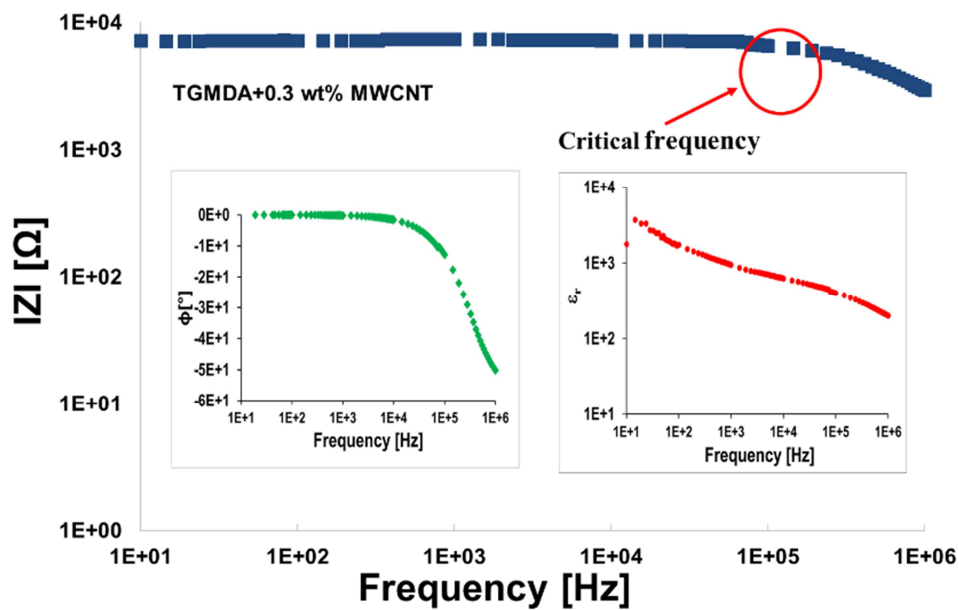


**FIGURE 5.** Modulus of impedance as function of frequency. Red circle highlights the critical frequency, i.e.  $f_c$ , for such composite. The inset shows the relative phase (degree) and the dielectric permittivity of the specimen vs. frequency.

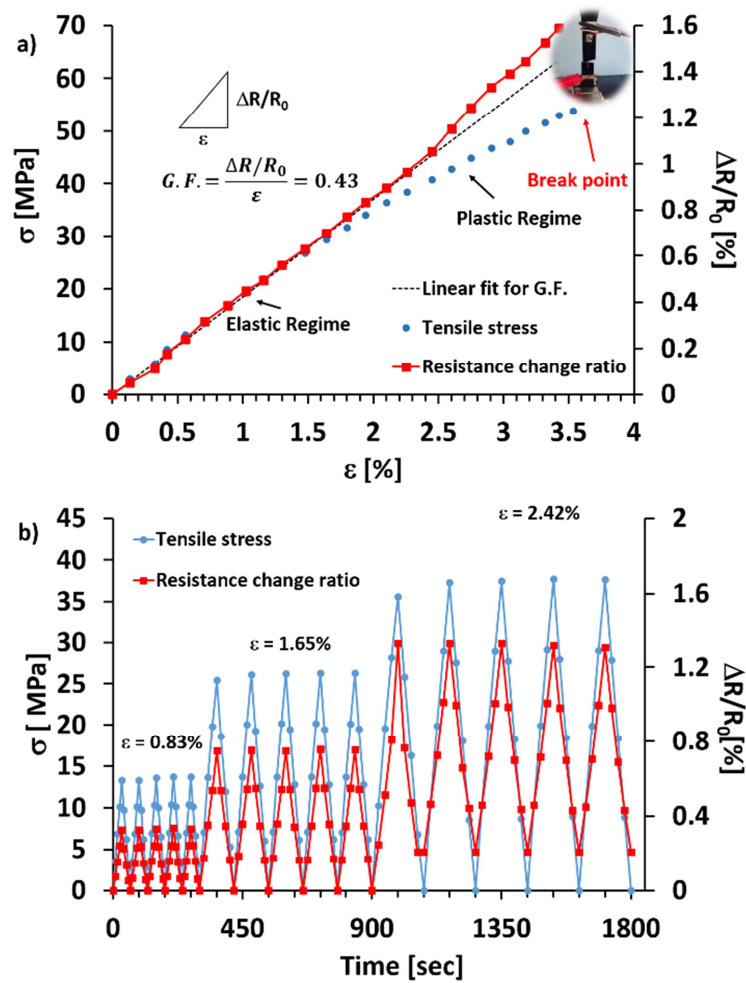


**Figure 6.** Mechanical behavior (i.e.  $\sigma$ , left vertical axis) and normalized change of electrical resistance (i.e.  $\Delta R/R_0$ , right vertical axis) observed in tensile stress as function of the axial strain ( $\epsilon$ ) and vs. time for cycling tension loading of nanocomposites, in fig. a) and b), respectively.

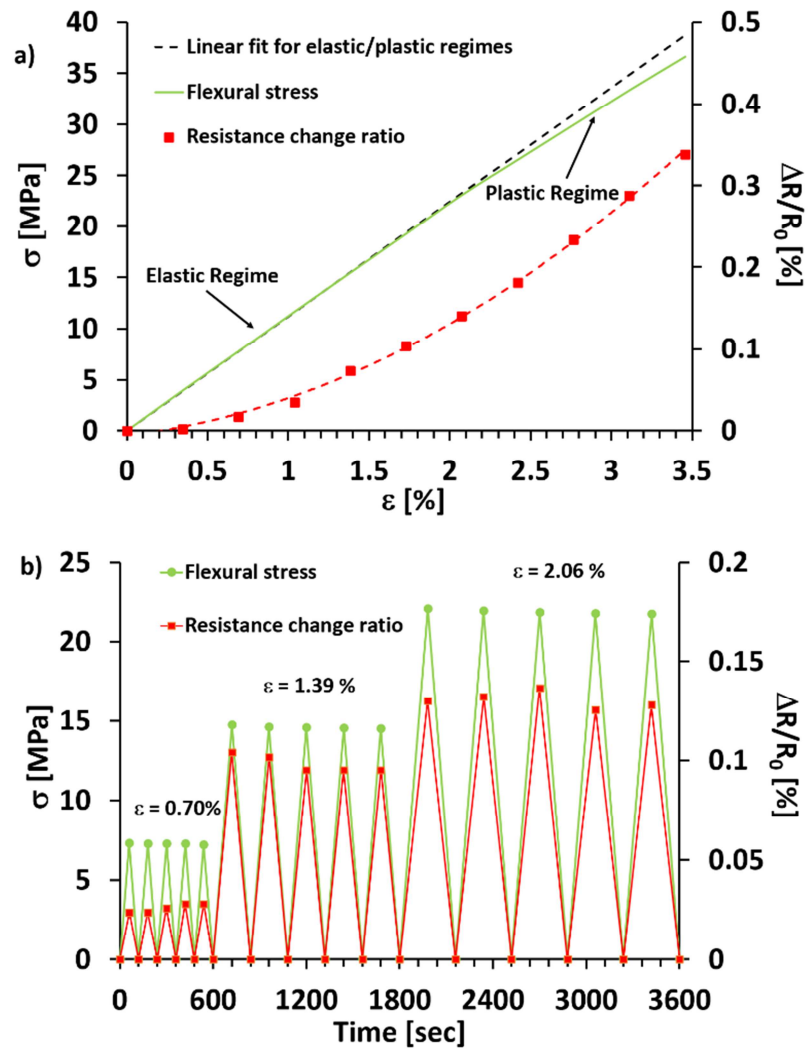


**FIGURE 7.** Mechanical behavior (i.e.  $\sigma$ , left vertical axis) and normalized change of electrical resistance (i.e.  $\Delta R/R_0$ , right vertical axis) observed in flexural stress as function of the axial strain ( $\epsilon$ ) and vs. time for cycling tension loading of nanocomposites, in fig. a) and b), respectively.

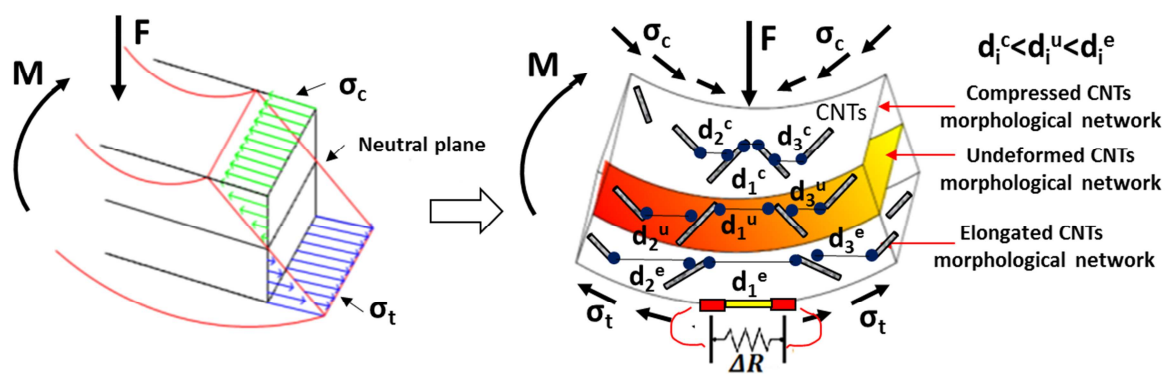


**FIGURE 8.** Dynamic deformation in the case of bending stress (left) and geometrical effect on the CNT morphological electrical network (right).

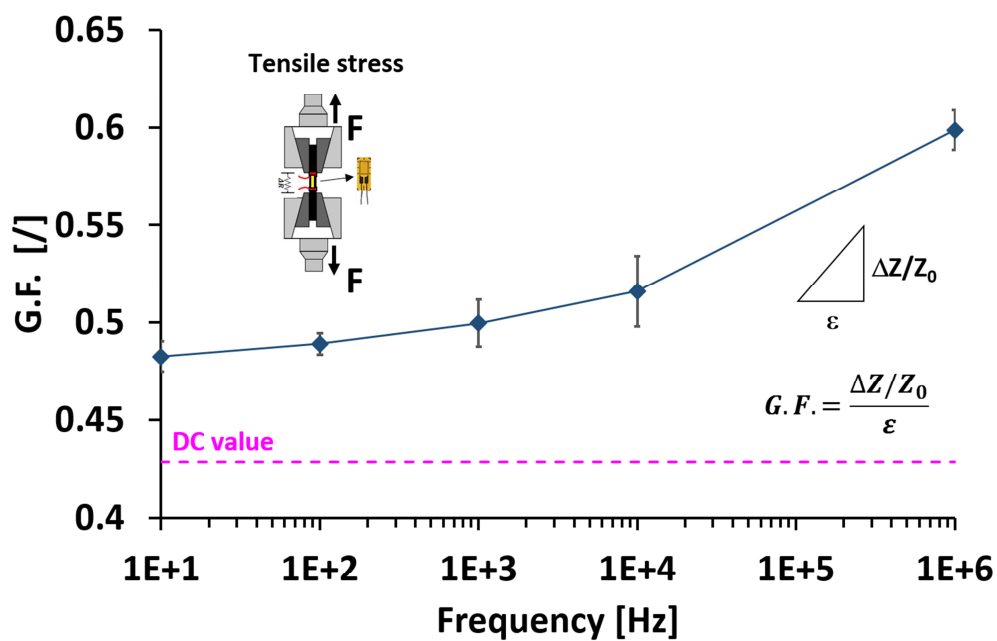


**FIGURE 9.** Sensitivity vs. frequency of the composite under tensile stress. The markers refer to the average value of the measurements carried out on different specimens. The corresponding error bars are also reported.

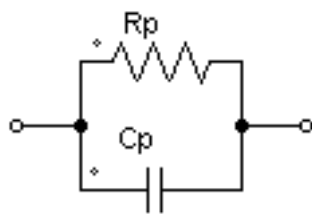


**FIGURE 10.** Equivalent circuit for the electrical behavior of a nanocomposite

ACCEPTED MANUSCRIPT

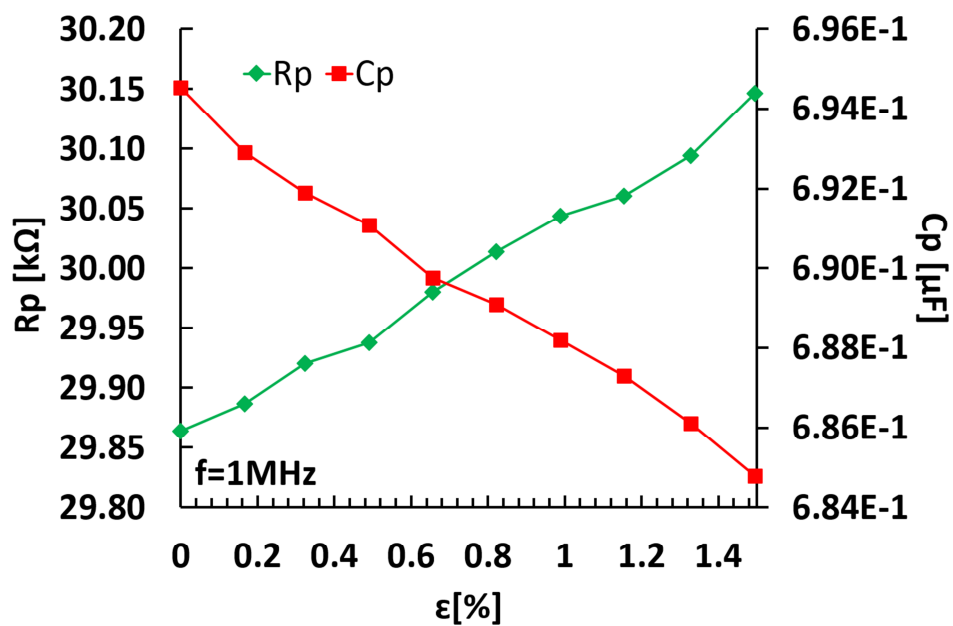


**FIGURE 11.** Resistance and capacitance variation of the sensor under different level of strain for composites analyzed at  $f=1\text{MHz}$ .

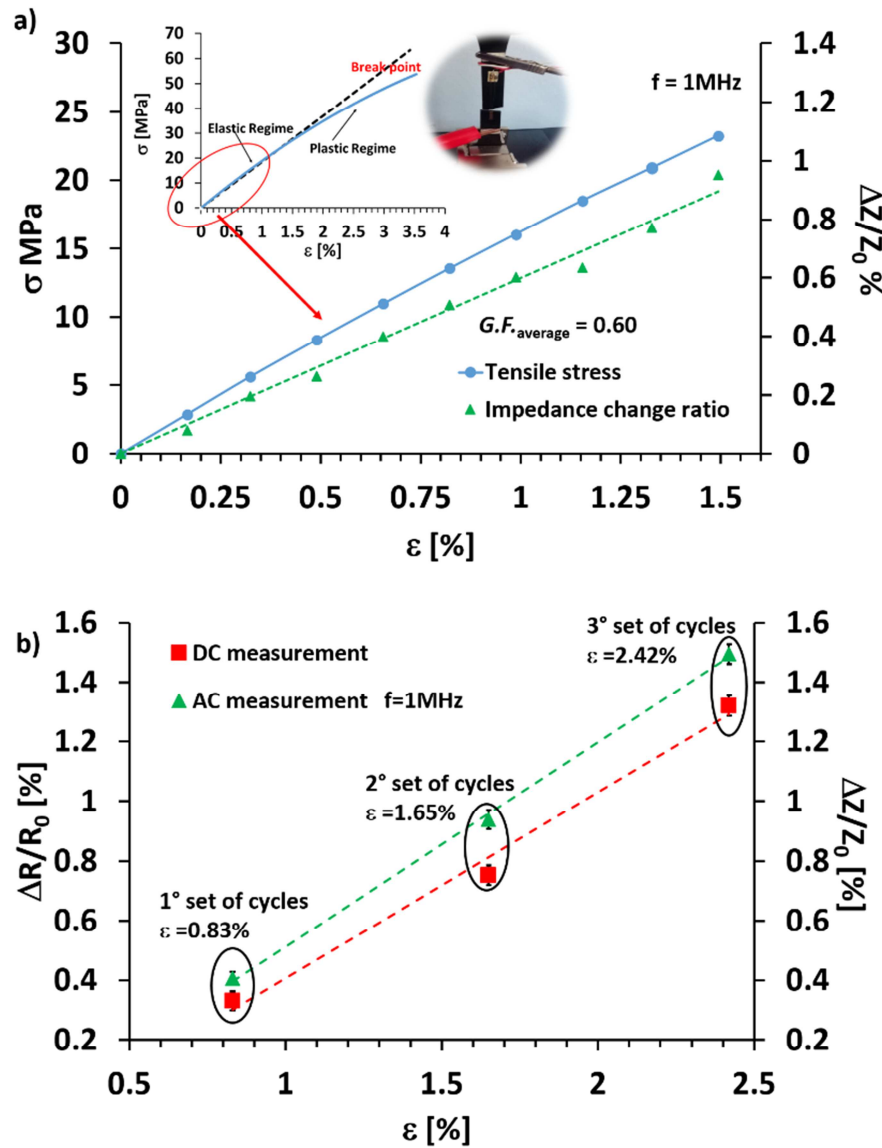


**Figure 12.** a) Sensitivity of the composite under tensile stress evaluated in the elastic range; b) Comparison of the sensitivity of the composite under tensile stress measured in DC and AC domain. The markers refer to the average value of the measurements performed on different specimens. The corresponding error bars are also reported.

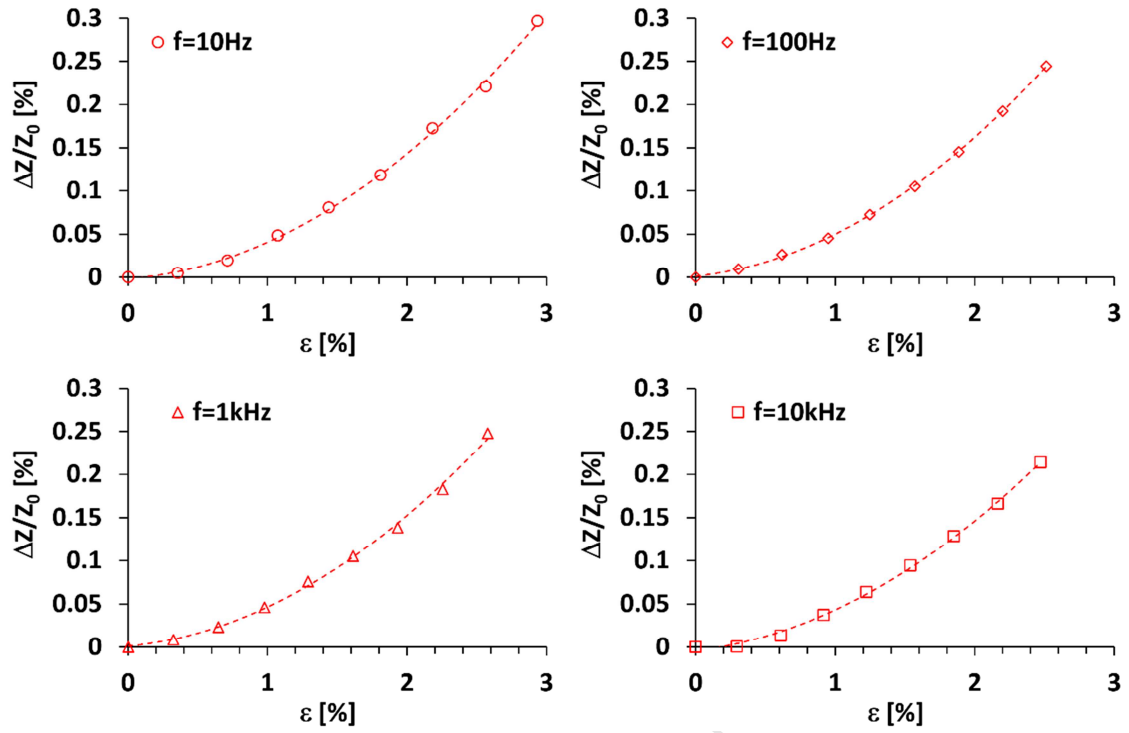


**Figure 13.** Behavior of normalized change of electrical impedance versus flexural stress at different operating frequency.

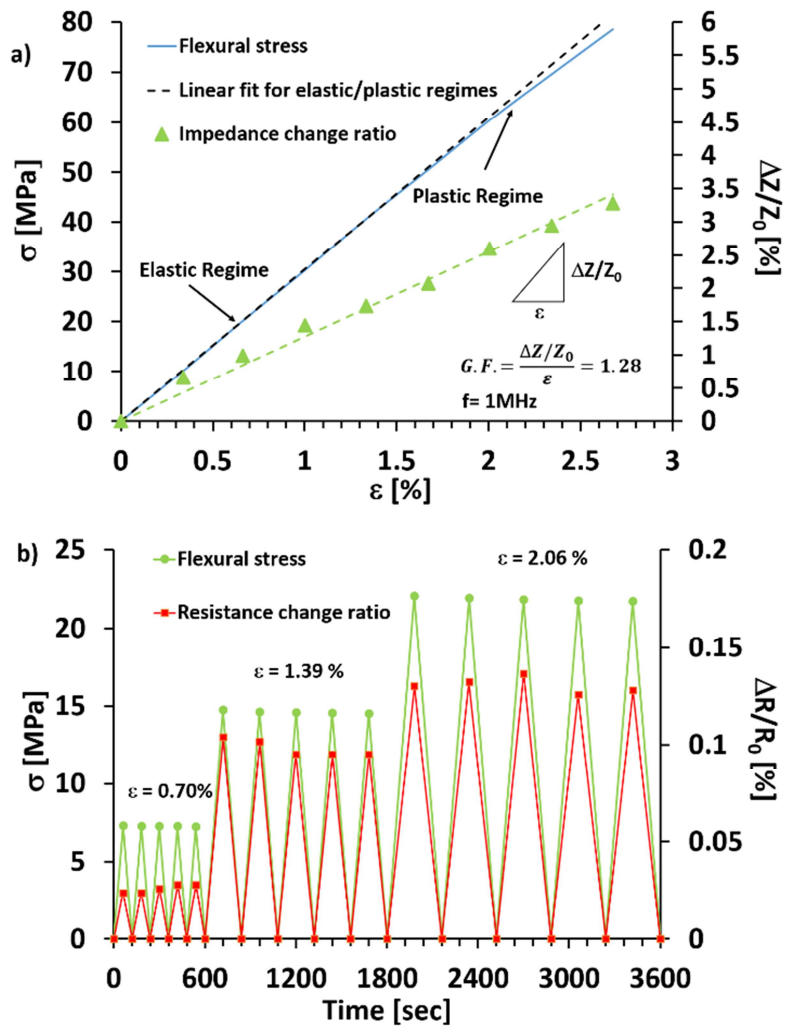


**Figure 14.** Mechanical behavior (i.e.  $\sigma$ , left vertical axis) and normalized change of impedance (i.e.  $\Delta Z/Z_0$ , right vertical axis) measured at the optimal operating frequency of 1MHz in flexural stress as function of the axial strain ( $\epsilon$ ) and vs. time for cycling tension loading of nanocomposites, in fig. a) and b), respectively.

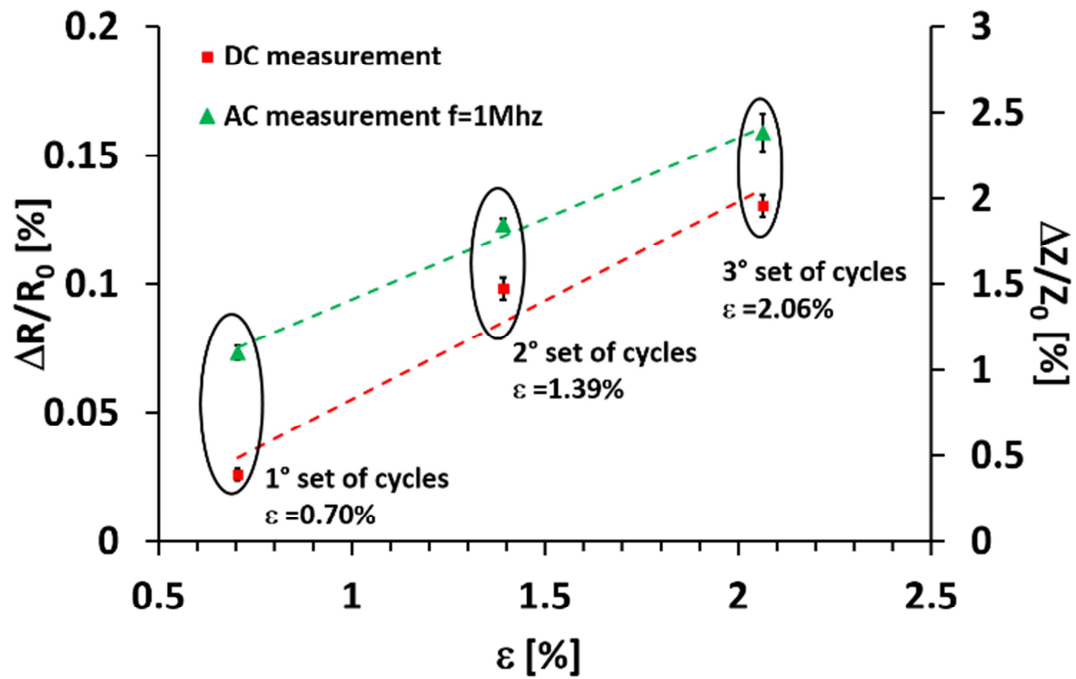


**Figure 15.** Comparison of the sensitivity to strain of the composite evaluated with DC and AC measurements. The markers refer to the average value of the measurements performed on different specimens. The corresponding error bars are also reported.